Pergamon

Int. J. Heat Mass Transfer. Vol. 38, No. 6, pp. 1033–1041, 1995

0017-9310/95 $9.50+0.00

0017-9310(94)00222-3

Heat and moisture transfer and hygrostress crack formation and propagation in cylindrical, elastoplastic food

MASAAKI IZUMI† and KAN-ICHI HAYAKAWA‡

New Jersey Agricultural Experiment Station, Department of Food Science, Cook College, Rutgers—The State University of New Jersey, P. O. Box 231, New Brunswick, NJ 08903, U.S.A.

(*Received* 13 *October* 1993 *and in final form* 7 *July* 1994)

Abstract—A finite element based method was developed to simulate hygrostress multiple crack formation and propagation in a cylindrical, elastoplastic food undergoing a simultaneous heat and moisture transfer process. Heat and moisture transfer was simulated using a model developed previously in the authors' laboratory, and hygrostress formation using a virtual work principle-based, incremental method. Criteria of critical, normal tensile stress and of crack-tip-opening angle were used to simulate hygrostress crack formation and propagation, respectively. The developed method was validated experimentally. Simulation results show temperature and moisture distributions were perturbed by multiple hygrostress crack formation and propagation.

INTRODUCTION

Many foods undergo drying processes, since dehydration is one of the key means of producing shelf-stable products. During these processes, hygrostresses are formed within the foods due to nonuniform shrinkage and without careful process controls this leads to stress crack formation and propagation. Since stress cracks in foods result in products of inferior quality, several researchers have developed simulation methods for heat and moisture transfer and hygrophysical changes to assist drying process optimization.

Misra and Young [1] were the first researchers to analyze moisture transfer, elastic hygrostrain and hygrostress formation in food (spherically approximated soybean). Litchfield and Okos [2] examined, using their predictive model, simultaneous heat and moisture transfer, viscoelastic hygrostrain and stress formation in a spherically approximated corn kernel undergoing drying, tempering and cooling processes. Haghighi and Segerlind [3, 4] developed a finite element model for estimating thermohygro viscoelastic stress and applied it to simulated transport processes and viscoelastic stress formation in spherical food. Tsukada *et al.* [5] developed a simulation method for simultaneous heat and moisture transfer and hygrostress formation in elastoplastic food of an axisymmetrically irregular shape. Laguë and Jenkins [6, 7] developed a method for modeling heat and moisture transfer and viscoelastic hygrostress formation and stress failure of axisymmetric food (rice).

The above published methods are useful to examine transient state transport processes and hygrophysical changes in biological material. However, no published method is available to simulate hygrostress crack propagation in food undergoing a heat and moisture transfer process. Therefore, the objective of the present work is to develop such a method applicable to food of a cylindrical shape undergoing a dehydration or hydration process.

MATHEMATICAL MODEL AND SIMULATION METHOD

Heat and moisture transfer

Heat and moisture transfer in food was simulated by equations developed in the author's laboratory [8] that include all thermodynamically interactive heat and mass fluxes and mass flux correction factors.

Moisture transfer:

$$(\partial c/\partial t) = -\mathrm{div}\{\mathbf{J}_m\} + \sum_j R_j. \quad (1)$$

Heat transfer:

$$C_p\rho_b(\partial T/\partial t) = -\mathrm{div}\{\mathbf{J}_h\} + \sum_j \Delta H_{vj}R_j + \Delta H_v\eta(\partial c/\partial t) \quad \text{for } t > 0 \text{ and } \vec{X} \in V. \quad (2)$$

The fluxes $\{\mathbf{J}_m\}$ and $\{\mathbf{J}_h\}$ are expressed below:

$$\{\mathbf{J}_m\} = -\beta_1 D_w \,\mathrm{grad}(C) - \beta_2 D_t \,\mathrm{grad}(T) - \beta_3 D_p \,\mathrm{grad}(p) \quad (3)$$

†Current affiliation: Department of Applied Chemistry and Molecular Science, Faculty of Engineering, Iwate University, Morioka 020, Japan.

‡Author to whom correspondence should be addressed.

NOMENCLATURE

$[\mathbf{A}]$ matrix defined by equation (20)
$\{\Delta\mathbf{a}\}$ vector of incremental displacements at all nodes in one finite element, Δu and Δv of each node are arranged alternately for all nodes as a 16-element vector [m]
a_w water activity
B Stefan–Boltzmann constant [W $(m^2\ K^4)^{-1}$]
$[\mathbf{B}]$ $= [\mathbf{A}][\mathbf{N}]$, strain–displacement matrix
b_f, b_p empirical constants for estimating location variable σ_c and δ_c, respectively
C volumetric moisture concentration [kg m^{-3}]
c_{fe}, c_{f0}, c_{f1} empirical parameters for estimating σ_c
C_m specific mass capacity [kg moisture (kg dry solid °M)$^{-1}$]
c_{pe}, c_{p0}, c_{p1} empirical parameters for estimating δ_c
C_p specific heat [J $(kg\ K)^{-1}$]
C_ϕ temperature coefficient [kg water (kg dry solid K)$^{-1}$]
CTA crack tip opening angle
CTD crack tip opening displacement
$[\mathbf{D}]$ $= [\mathbf{D}_{el}] + \zeta[\mathbf{D}_{pl}]$
$[\mathbf{D}_{el}]$ elastic strain–stress tensor
D_p pressure mass diffusivity [kg $(m\ s\ Pa)^{-1}$]
$[\mathbf{D}_{pl}]$ plastic strain–stress tensor
D_t soret mass diffusivity [kg $(m\ s\ K)^{-1}$]
D_w mass diffusivity (concentration gradient based) [$m^2\ s^{-1}$]
$\{\Delta\mathbf{d}\}$ vector of incremental displacement at any location
E Young's modulus [Pa]
$\{\mathbf{e}_n\}$ outward normal unit vector
G shear modulus [P_a]
H strain-hardening rate [Pa]
ΔH_{rj} rate of heat generated or consumed by chemical reaction [W m^{-3}]
ΔH_v latent heat of phase change [J m^{-3}]
h_m convective surface mass transfer coefficient [kg $(m^2\ s\ Pa)^{-1}$]
h_t convective surface heat transfer coefficient [W $(m^2\ K)^{-1}$]
$\{\mathbf{J}_h\}$ heat flux [W m^{-2}]
$\{\mathbf{J}_m\}$ moisture flux [kg $(m^2\ s)^{-1}$]
k_c Dufour thermal conductivity [W $m^2\ kg^{-1}$]
k_p pressure thermal conductivity [W $(m\ Pa)^{-1}$]
k_t thermal conductivity (temperature gradient based) [W $(m\ K)^{-1}$]
L parameter in GAB equation
m sensible heat index for Dufour heat flux
$[\mathbf{N}]$ shape functions of all nodes in one finite element arranged as a 2×16 matrix applicable to $\{\Delta\mathbf{a}\}$
n sensible heat induced for pressure heat flux
p water vapor pressure [Pa]
Q parameter in Gingenheim–Anderson–de Bore equation
R universal gas constant [kJ $(mol\ K)^{-1}$]
R_j reaction rate [kg $(s\ m^3)^{-1}$]
r radial distance variable [m]
S food surface
S_v volumetric shrinkage coefficient; ratio of current volumetric element to the initial volumetric element
T temperature [°C]
T_k temperature [K]
t time [s]
Δu incremental displacement in the r-direction at any location, an element of $\{\Delta\mathbf{d}\}$ [m]
V volume or space occupied by food except its surface [m^3]
Δv incremental displacement in the z-direction at any location, an element of $\{\Delta\mathbf{d}\}$
W moisture content [kg water (kg solid)$^{-1}$]
W_m food moisture equilibrated to 100% humidity (temperature-dependent) [g water (g dry solid)$^{-1}$]
W_{mi} food moisture equilibrated to 0% humidity (temperature-dependent) [g water (g dry solid)$^{-1}$]
W_n parameter in GAB equation [g water (g dry solid)$^{-1}$]
$\vec{X}$ spacial coordinates
z axial variable in cylindrical coordinates [m].

Greek symbols
β_1, β_2, β_3 mass flux correction factors introduced by Furuta and Hayakawa [8]
γ magnitude of observed total shear strain
γ_s magnitude of elastoplastic shear strain
γ_1, γ_2, γ_3 empirical parameters [8] for relating a static pressure change with vaporized or condensed water mass, volumetric shrinkage and temperature change, respectively
δ_c critical crack tip opening angle [°]
ε magnitude of observed normal strain with the orientation represented by the subscript
ε_s magnitude of elastoplastic normal strain with the orientation represented by the subscript

$\{\Delta\varepsilon\}$ vector of incremental observed strains, see equation (19)
$\{\Delta\varepsilon_s\}$ vector of incremental elastoplastic strain
$\{\Delta\varepsilon_0\}$ vector of incremental stress free strains
ζ yield stress parameter defined by equation (26)
η Luikov's phase convergency criterion
θ angular variable
λ random variates of rectangular distribution whose values are between 0 and 1 and which are assigned to different axial location
μ_0 Gibbs free energy of saturated free water [J mol^{-1}]
ν Poisson's ratio
ξ_f random variates of rectangular distribution whose values are between $-b_f$ and b_f, they are assigned to different axial location
ξ_p random variates of rectangular distribution whose values are between $-b_p$ and b_p, they are assigned to different axial location
ρ_b bulk density of bone dry solid [kg m^{-3}]
σ magnitude of normal stress, orientation represented by subscript [kN m^{-2}]
$\bar{\sigma}$ equivalent stress (scalar) [kN m^{-2}]
σ_c magnitude of critical tensile stress for crack formation [kN m^{-2}]
σ' magnitude of deviatoric stress [kN m^{-2}]
$\{\boldsymbol{\sigma}\}$ stress vector whose components are in cylindrical coordinate direction
$\{\boldsymbol{\sigma}_p\}$ principal stress vector estimated from $\{\boldsymbol{\sigma}\}$
$\{\Delta\boldsymbol{\sigma}\}$ incremental stress vector
τ magnitude of shear stress [kN m^{-2}]
ϕ mass transfer potential [°M]
Ω product of emissivity and shape factor for radiative heat exchange.

Subscripts
a ambient
fc critical value for crack formation
n normal to surface
e equilibrium
0 initial
pc critical value for crack propagation
r r-direction in cylindrical coordinate
s surface
z z-direction in cylindrical coordinate
θ θ-direction in cylindrical coordinate
ϕ mass transfer potential.

$$\{\mathbf{J}_h\} = -k_t \operatorname{grad}(T) - (-1)^m k_c \operatorname{grad}(C) - (-1)^n k_p \operatorname{grad}(p). \quad (4)$$

In equations (3) and (4), grad(p) is correlated as follows:

$$\operatorname{grad}(p) = \gamma_1 \eta \operatorname{grad}(C) - \gamma_2 \operatorname{grad}(S_v) + \gamma_3 \operatorname{grad}(T). \quad (5)$$

The initial and boundary conditions are:

I.C.:

$$C = C_0 \quad T = T_0 \quad \text{for } t = 0 \quad \text{and } \vec{X} \in S \cup V \quad (6)$$

B.C.:

$$h_m(p_a - p_s) = \{\mathbf{e}_n\}\{\mathbf{J}_m\} \quad (7)$$

$$h_t(T_a - T_s) + B\Omega(T_a^4 - T_s^4) - h_m(1-\eta)\Delta H_v(p_a - p_s) = \{\mathbf{e}_n\}\{\mathbf{J}_h\} \quad \text{for } t > 0 \quad \text{and } \vec{X} \in S. \quad (8)$$

Since moisture concentration C was not mass transfer potential [9, 10], it was converted to a proper potential for better understanding of a transport process, a potential based on the Gibbs free energy of moisture in food [11]:

$$\phi = \begin{cases} \mu_0 + \mathrm{R}T_k \ln a_w & \text{for } W \leqslant W_m \\ \{(W - W_m)/(W_m - W_{mi}) + 1\}\mu_0 & \text{for } W > W_m. \end{cases} \quad (9)$$

Temperature and moisture dependent water activity, a_w, in the above equation was estimated by the GAB (Gugenheim–Anderson–de Bore) moisture sorption isotherm equation, equation (10), since this equation estimates accurately moisture sorption isotherms of food [12],

$$W = W_n QLa_w / \{(1 - La_w)(1 - La_w + QLa_w)\}. \quad (10)$$

The volumetric concentration, C, in equations (1)–(6) is transformed to the dry mass based concentration, W, by

$$C = \rho_b W = (\rho_{b0}/S_v) W. \quad (11)$$

Moisture equilibrated within a volumetric element in food depends on temperature and mass transfer potential. Therefore, one has

$$\mathrm{d}W = (\partial W/\partial\phi)_T \,\mathrm{d}\phi + (\partial W/\partial T)_\phi \,\mathrm{d}T = C_m \,\mathrm{d}\phi + C_\phi \,\mathrm{d}T. \quad (12)$$

Dependent variable C in equations (1)–(8) was transformed to ϕ using equations (9)–(12). For example,

$$\mathrm{d}C = (\rho_{b0}/S_v)\{(W/S_v)(\mathrm{d}S_v/\mathrm{d}W) + 1\}(C_m \,\mathrm{d}\phi + C_p \,\mathrm{d}T).$$

It should be noted that S_v of most foods depends only on food moisture.

The above equations were solved by the Galerkin's finite element method using curved side, eight-node

quadratic isoparametric elements, since this use simplified fitting curved crack surfaces. (Interactively solved equations for hygrophysical changes are given below.)

Finite element descretization produced simultaneous, nonlinear first-order ordinary differential equations. These equations were solved by the Crank–Nicholson method.

Hygrostrain–stress formation

Food may be approximated as elastoplastic within a small strain region. Therefore, the present work assumed elastoplasticity. Since the material property equations were nonlinear, an incremental method [13, 14] was used to estimate transient state strain–stress distributions. Transient state hygrostrain–stress formation was estimated interactively using finite element solutions of the heat and mass transfer equation (coupled solutions). The following equations show Galarkin's finite element-based governing equations for the stress–strain field in an elastoplastic body:

Local strain change during time increment

$$\{\Delta\varepsilon\} = \{\Delta\varepsilon_s\} + \{\Delta\varepsilon_0\} \tag{13}$$

Principle of minimum virtual work energy

$$\int_v [\mathbf{B}]^T[\mathbf{D}][\mathbf{B}]\,dv\{\Delta\mathbf{a}\} = \int_v [\mathbf{B}]^T[\mathbf{D}]\{\Delta\varepsilon_0\}\,dv \tag{14}$$

Strain–displacement relation

$$\{\Delta\varepsilon\} = [\mathbf{A}]\{\Delta\mathbf{d}\} \tag{15}$$

Stress–strain relation

$$\{\Delta\sigma\} = [\mathbf{D}]\{\Delta\varepsilon_s\} = ([\mathbf{D}_{el}] + \zeta[\mathbf{D}_{pl}])\{\Delta\varepsilon_s\}. \tag{16}$$

$\{\Delta\mathbf{d}\}$, $\{\Delta\varepsilon\}$, $\{\Delta\varepsilon_s\}$, $\{\Delta\varepsilon_0\}$ and $\{\Delta\sigma\}$ are vectorial expressions of incremental displacement total (observed) strain, elastoplastic strain, stress free hygroshrinkage strains and stress tensors, respectively:

$$\{\Delta\mathbf{d}\} = \begin{Bmatrix}\Delta u\\ \Delta v\end{Bmatrix} \tag{17}$$

$$\{\Delta\sigma\} = \begin{Bmatrix}\Delta\sigma_r\\ \Delta\sigma_z\\ \Delta\sigma_\theta\\ \Delta\tau_{rz}\end{Bmatrix} \tag{18}$$

$$\{\Delta\varepsilon\} = \begin{Bmatrix}\Delta\varepsilon_r\\ \Delta\varepsilon_z\\ \Delta\varepsilon_\theta\\ \Delta\gamma_{rz}\end{Bmatrix} \quad \{\Delta\varepsilon_s\} = \begin{Bmatrix}\Delta\varepsilon_{sr}\\ \Delta\varepsilon_{sz}\\ \Delta\varepsilon_{s\theta}\\ \Delta\gamma_{srz}\end{Bmatrix}$$

$$\{\Delta\varepsilon_0\} = \begin{Bmatrix}\Delta S_v^{1/3}\\ \Delta S_v^{1/3}\\ \Delta S_v^{1/3}\\ 0\end{Bmatrix}. \tag{19}$$

[A] is a matrix defined by

$$[\mathbf{A}] = \begin{Bmatrix}\partial/\partial r & 0\\ 0 & \partial/\partial r\\ 1/r & 0\\ \partial/\partial z & \partial/\partial r\end{Bmatrix}. \tag{20}$$

$[\mathbf{D}_{el}]$ and $[\mathbf{D}_{pl}]$ are elastic and plastic stress–strain matrices, respectively:

$$[\mathbf{D}_{el}] = \frac{E(1-v)}{(1+v)(1-2v)}\begin{Bmatrix}1 & \frac{v}{1-v} & \frac{v}{1-v} & 0\\ & 1 & \frac{v}{1-v} & 0\\ & & 1 & 0\\ & & & \frac{1-2v}{2(1-v)}\end{Bmatrix}$$

symmetric tensor (21)

$$[\mathbf{D}_{pl}] = -\frac{1}{\frac{\bar\sigma^2 H}{9G^2} + \frac{\bar\sigma^2}{3G}}\begin{Bmatrix}\sigma_r'^2 & \sigma_r'\sigma_z' & \sigma_r'\sigma_\theta' & \sigma_r'\tau_{rz}\\ & \sigma_z'^2 & \sigma_z'\sigma' & \sigma_z'\tau_{rz}\\ & & \sigma_\theta'^2 & \sigma_\theta'\tau_{rz}\\ & & & \tau_{rz}^2\end{Bmatrix}$$

symmetric tensor (22)

where G is the shear modulus defined as

$$G = E/2(1+v). \tag{23}$$

σ_r', σ_z' and σ_θ' are deviatoric stresses defined as

$$\left.\begin{aligned}\sigma_r' &= (2\sigma_r - \sigma_z - \sigma_\theta)/3\\ \sigma_z' &= (2\sigma_z - \sigma_\theta - \sigma_r)/3\\ \sigma_\theta' &= (2\sigma_\theta - \sigma_r - \sigma_z)/3\end{aligned}\right\}. \tag{24}$$

$\bar\sigma$ is the equivalent stress defined as

$$\bar\sigma = [0.5\{(\sigma_r-\sigma_z)^2 + (\sigma_z-\sigma_\theta)^2 + (\sigma_\theta-\sigma_r)^2 + 6\tau_{rz}^2\}]^{1/2}. \tag{25}$$

A yield stress parameter ζ in equation (16) is $\bar\sigma$ dependent as follows:

$$\begin{aligned}&\zeta = 0 \text{ when } \bar\sigma < \sigma_d \text{ for any } \bar\sigma\,d\bar\sigma\\ &\quad\text{or when } \bar\sigma > \sigma_d \text{ and } \bar\sigma\,d\bar\sigma < 0\\ &\zeta = 1 \text{ when } \bar\sigma > \sigma_d \text{ and } \bar\sigma_d\bar\sigma > 0.\end{aligned} \tag{26}$$

The total incremental displacement vector $\{\Delta\mathbf{a}\}$ at each finite element node was estimated by equation (14). The total strain vector at any location may be estimated using finite element nodal shape functions:

$$\{\Delta\varepsilon\} = [\mathbf{A}][\mathbf{N}]\{\Delta\mathbf{a}\} = [\mathbf{B}]\{\Delta\mathbf{a}\}. \tag{27}$$

The shape functions, [N], of the isoparametric element are given in most reference books on finite element methods [equation (14)]. Incremental elastoplastic strains $\{\Delta\varepsilon_s\}$ were estimated by equation (13) and finally incremental stress $\{\Delta\sigma\}$ by equation (16). Current hygrostrains and stresses were obtained by adding $\{\Delta\varepsilon\}$ and $\{\Delta\sigma\}$ to those at the previous time increment.

Principal stresses $\{\sigma_p\}$ were estimated at each node by determining the characteristic values and vectors of nodal stresses after expressing them in a tensorial form.

Hygrostress crack formation and propagation

Many dried foods are brittle. A critical normal tensile stress (tensile principal stress) has been used as a failure criterion for such material. Additionally, Tsukada *et al.* [5] observed that hygrostress crack formation in sample food was related closely to the magnitude of principal, tensile stress and that the orientation of hygrostress crack was orthogonal to the orientation of the critical, principal, tensile stress. Therefore, it was assumed that a stress crack was formed at the location where a principal, tensile hygrostress exceeded a critical level, σ_c, and that the crack orientation was orthogonal to this hygrostress.

According to preliminary experimental work, the critical stress level was independent of temperature within a normal temperature range for food drying (20–65°C) and of W in a high range. The critical level increased when food moisture was reduced below certain moisture concentration, W_c. Additionally, there are likely location-to-location variations in σ_c in the z-direction, since most cylindrical foods are made through extrusion processes. Based on this observation, the following relationship was assumed:

$$\sigma_c = \begin{cases} (1+\xi_f)(C_{f0}-C_{f1}W) & \text{for } W_{mi} \leqslant W \leqslant W_{fc} \\ (1+\xi_f)C_{fe} & \text{for } W_{fc} \leqslant W \end{cases} \tag{28}$$

where $C_{fe} = C_{f0} - C_{fi}\, W_{fc}$ and $\xi_f = b_f(2\lambda - 1)$.

In the above, λ is a random variate of a rectangular distribution between 0 and 1. One variate is assigned randomly to each node in the axial direction.

There are several criteria for crack propagation, e.g. criteria of crack tip stress, energy release rates, tearing modulus, J-integral, and crack-tip-opening-displacement (COD) or -angle (COA) [15, 16]. All of these methods, except COD and COA, are applicable only to the propagation of one crack, not to multiple crack propagation. Therefore, the COA method was used for the present work.

According to a simulation method based on the COA, a hygrostress crack propagates along one side length of a finite element when a COA exceeds a critical angle, δ_c. Many foods become more brittle in a low moisture region, while they are less brittle in a high moisture region. Therefore, δ_c is small for low W and δ_c increases for high W. Additionally, there are likely z-directional variations in δ_c as in σ_c. Based on this, equation (29) was assumed.

$$\delta_c = \begin{cases} (1+\xi_p)c_{pe} & \text{for } W_{mi} \leqslant W \leqslant W_{pc} \\ (1+\xi_p)(C_{p0}+c_{p1}W) & \text{for } W_{pc} \leqslant W \end{cases} \tag{29}$$

where $C_{pc} = c_{p0} + c_{p1}\, W_{pc}$ and $\xi_p = b_p(2\lambda - 1)$.

The COA criterion is incorporated into the finite element method as follows: an abridged computer program flow chart in Fig. 1. A sample body is subdivided into finite elements of two types: elements for simulating hygrostress crack formation propagation [Bs of Fig. 2(a)] and those of standard elements for analyzing heat and moisture transfer and hygrostress formation [As of Fig. 2(a)]. Element B was also used

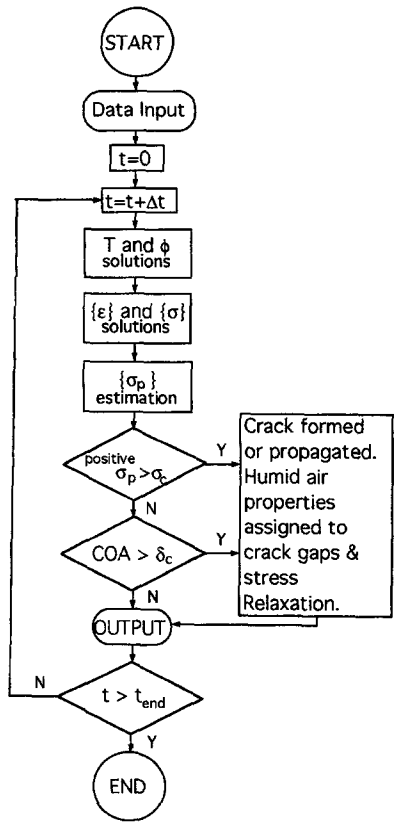

Fig. 1. Abridged flow chart of prepared computer program.

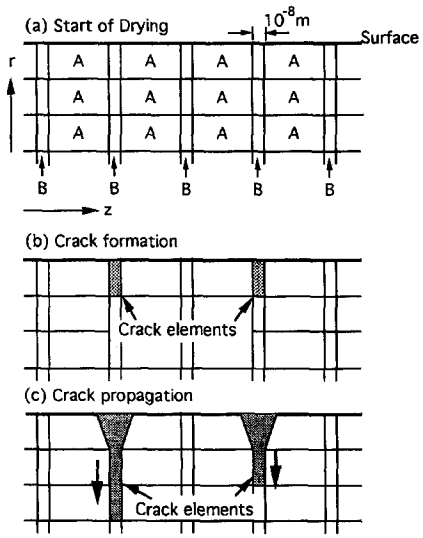

Fig. 2. Finite elements for hygrostress crack formation and propagation.

for the heat and moisture transfer analysis until crack formation or propagation. The side dimension of each element B in the z-direction is extremely small (10^{-8} m for the present work). A crack of width 10^{-8} m is formed along the r-direction of a B-element, when tensile, principal stress in the z-direction reaches the critical level, equation (28) [Fig. 1(b), the maximum tensile principal stress occurring in the z-direction according to a preliminary analysis]. When a crack is formed, a cracked B-element is filled with stationary, humid air equilibrated to temperature and moisture of surrounding A-elements. A crack propagates by one r-directional side dimension of the adjacent B-element, when a crack-tip-opening angle reaches a critical angle, equation (29) [Fig. 1(c)].

It should be noted that type B elements were placed initially along the axial sides of each element in addition to those shown in Fig. 1. However, the former elements were eliminated to save computer time, since principal, tensile stresses of the radial orientation were less than those of the axial orientation according to preliminary simulations (probably no cracks in the axial direction), and since most cracks were in the radial direction according to preliminary drying experiments.

EXPERIMENTAL

Drying experiments were conducted to validate the above described simulation method. For this, cyl-

Table 1. Drying conditions and physical mechanical properties for the simulation

Air temperature (T_a) : 55 [°C]
Initial sample temperature (T_0) : 25 [°C]
Initial sample moisture (W_0) : 0.4 [kg water (kg solid)$^{-1}$]
Relative humidity : 0.11
Surface heat transfer coefficient (h_t) : 23.2 [W m^{-2} K^{-1}]
Surface mass transfer coefficient (h_m) : 0.0685 [kg m^{-2} kPa^{-1} s^{-1}]
Volumetric shrinkage coefficient (S_v) :

$$S_v = 0.8798 + 0.601(W - 0.2)$$

Moisture diffusivity (D_w) :

$$D_w = 1.448 \times 10^{-4}(6.402 \times 10^{-4} + 10W^{-3})^2 W^{0.5954} \exp[8 \times 10^4(0.147 + 1/(1+10W))(1/323 - 1/(T+273))/8.314] \text{ [m}^2\text{ s}^{-1}\text{]}$$

Soret mass diffusivity (D_t) : 0.0 [kg m^{-1} s^{-1} K^{-1}]
Pressure mass diffusivity (D_p) : 0.0 [s]
Thermal conductivity (k_t) :

$$k_t = 0.35 + 1.16 \times 10^{-3}(T - 273) + 0.058W/(1+W) \text{ [W m}^{-1}\text{ K}^{-1}\text{]}$$

Dufour thermal conductivity (k_c) : 0.0 [W m^2 kg^{-1}]
Filtrational thermal conductivity (k_p) : 0.0 [W m^{-1} Pa^{-1}]
Luikov's phase conversion criteria (ϵ) :

$$\epsilon = 1 - W/W_0$$

Specific heat (C_p) :

$$C_p = 1.90 \times 10^3 - 12.1(T - 273) + 1.73 \times 10^3 W/(1+W) \text{ [J kg}^{-1}\text{ K}^{-1}\text{]}$$

Chemical reaction rate (R_j) : 0.0 [kg s^{-1}]
GAB isotherm

$$W_e = W_n Q L a_w / [(1 - La_w)(1 - La_w + QLa_w)] \text{ [kg water (kg solid)}^{-1}\text{]}$$

$$Q = 7.198 \times 10^{-4} \exp(302/T)$$

$$L = 0.370 \exp(142.1/T)$$

$$W_n = 0.07259 \exp(162.6/T)$$

Vapor pressure on the surface (P_s) :

$$P_s = 101.3 \times 10^3 a_w \exp[13.087(1 - 273.15/T)] \text{ [Pa]}$$

Hygrostress crack formation and propagation

$$\sigma_c = \begin{cases} (1+\xi_f)(1501 - 4947W) & \text{for } 0 \leqslant W \leqslant 0.289 \\ (1+\xi_f)71.3 & \text{for } 0.289 \leqslant W \end{cases}$$

$\xi_f = 0.04(2\lambda - 1)$ λ = random variate between 0 and 1

$$\delta_c = \begin{cases} (1+\xi_p)0.00025 & \text{for } 0 \leqslant W \leqslant 0.0289 \\ (1+\xi_p)(0.00043 + 0.00714W) & \text{for } 0.289 \leqslant W \end{cases}$$

$\xi_p = 0.04(2\lambda - 1)$ λ = random variates between 0 and 1

indrical samples (10 mm diameter × 200 mm length) were prepared from high amylose starch powder hydrate using plaster molds. Each of two samples had an installed, copper–constantan thermocouple (36 gauge wires) at the center to monitor temperature during drying. Samples were dried in a pilot plant forced air drying (C. G. Sargent's Son Corp., Granitville, MA). Weight changes of three samples were monitored periodically by an analytical balance. Additionally, separate samples were taken from the dryer through a sampling window at three different times (0.05, 0.1 and 0.5 h) for photographic observation of the stress crack.

The three samples used for monitoring the weight changes were subjected to dry matter (solid mass) determination by a vacuum oven method [17]. The crack observation samples were bisected carefully and cracks on the bisected surface were photographically recorded using a stereomicroscope.

The drying experiments were duplicated. The parametric values of σ_c and δ_c were estimated by comparing simulation results with those of one drying experiment.

For the simulation, half of a bisected sample face, 20 mm initial length × 5 mm initial radius, was subdivided into 100 type A finite elements by dividing both the z- and r-dimensions into 10. The crack propagation elements, type B elements, were placed between each of two adjacent type A elements in the radial direction (each element size 10^{-8} m in the z-direction × 0.5 mm in the r-direction, initial dimensions).

RESULTS AND DISCUSSION

Experimentally determined temperature and moisture concentration histories and stress crack formation and propagation were compared with those obtained through simulation using the above described model. All physical and transport properties except σ_c and δ_c parameters were obtained from published papers [11] (Table 1).

Experimentally determined central temperature and average moisture concentration histories agree well with simulated results, as shown in Fig. 3.

Figure 4(a) and (b) compares photographically observed hygrostress crack formation and propagation with simulated results. Figure 4(a) shows two principal stresses on the bisected face. The third principal stresses were orthogonal to those two and their magnitudes were less than those shown in Fig. 6(a) (three principal stresses at any location). The circular images of the photographs in Fig. 4(b) were due to the image field of the microscope. The central axis of the sample is in the middle of the image field, as indicated in Fig. 4(b).

There is a good agreement of the relative magnitudes of stress cracks between observed and simulated results. Stress cracks of significant sizes were formed on the exposed surface within 0.05 h. In an

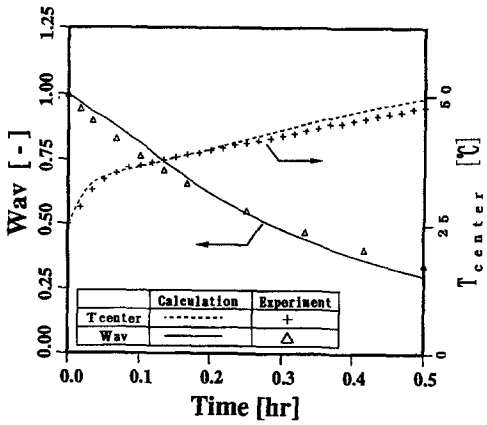

Fig. 3. Temperature and moisture concentration histories of cylindrical samples prepared from high amylose starch powder hydrate (5 mm diameter × 200 mm long initial dimensions).

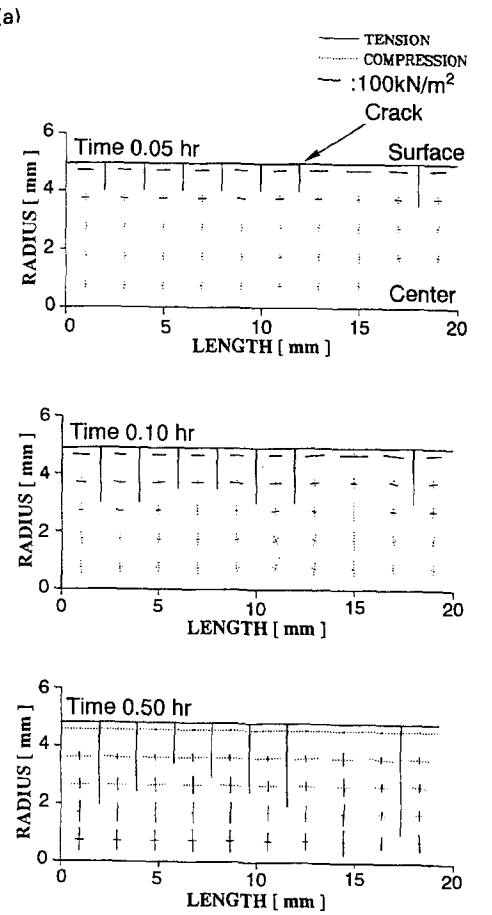

Fig. 4. Comparisons between simulated (a) and observed (b) cracks formed on half of an axially bisected sample face at 0.05, 0.1 and 0.5 h. Figure 4 shows two principal stresses acting on the bisected face (only one when the other is too small to be shown). Solid and dot bars in the simulation figure are principal tensile and compressional stresses, respectively, applicable at the intersection of a pair of bars or the mid-point of a bar. Stress magnitude and orientation are represented by bar length and orientation, respectively. Bars extending from the exposed surface are hygrostress cracks.

(b)

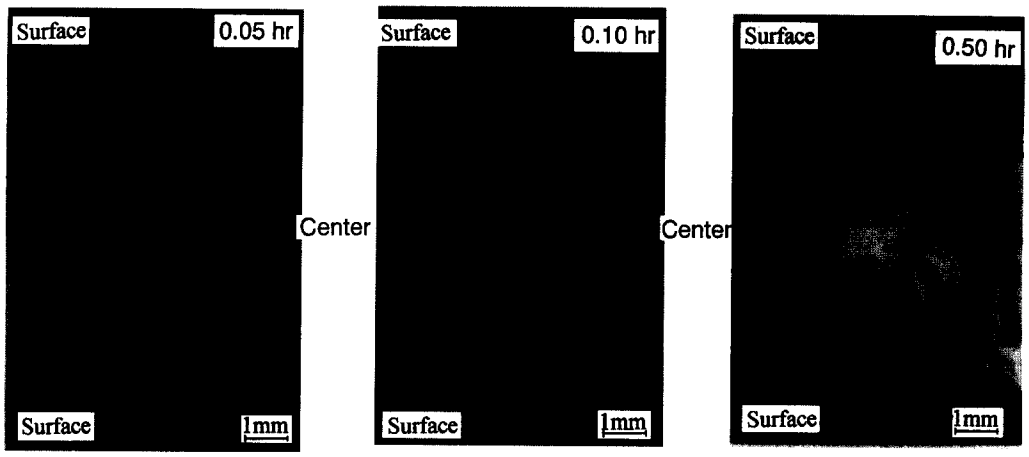

Fig. 4—*continued.*

early stage of drying, surface moisture was reduced, while there was no moisture reduction in the interior. This resulted in large hygrostrains forming on the surface, resulting in large tensile stress formation. Therefore, stress cracks were formed on the surface within a short drying time. It is of interest to note that the location of large tensile stresses moved inward with progress in drying.

Predicted moisture distributions at 0.016, 0.1 and 0.5 h of drying are shown in Fig. 5. Figure 5 shows

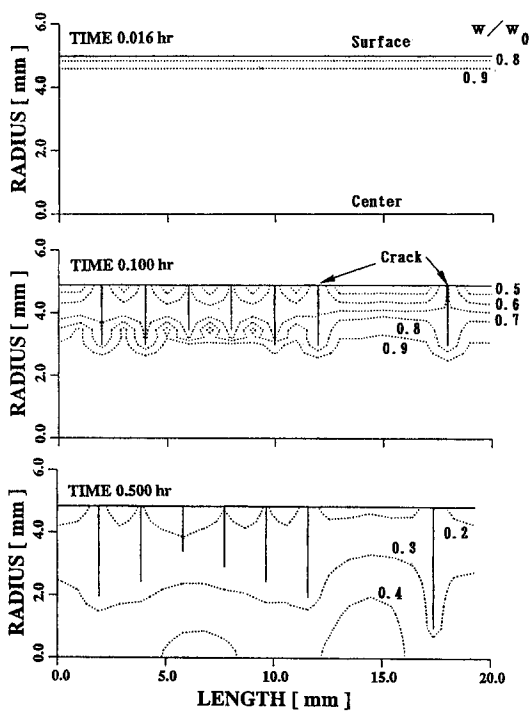

Fig. 5. Simulated moisture distributions on bisected face of a cylindrical sample made from high amylose starch powder hydrate at 0.016, 0.1 and 0.5 h of drying.

that, at 0.016 h, the influence of drying remained in a zone near the surface without any stress crack formation and all iso-concentration lines were parallel. However, at 0.1 h, irregular concentration distribution occurred around the cracks because of faster moisture transfer through the cracks. This implies that moisture transfer in food with cracks cannot be estimated accurately without considering crack formation and propagation. Additionally, this change of moisture distribution after crack formation influenced stress formation due to changes in hygrostrains.

At 0.5 h, cracks ceased to propagate due to no additional shrinkage, because of low moisture content and due to the influence of moisture content on σ_c and δ_c.

Figure 6 shows predicted temperature distributions at the same drying times. Temperature distribution lines at 0.016 h were parallel to the exposed surface like the moisture distribution. However, the thermal influence extended further to the interior due to a greater heat transfer rate compared to moisture transfer rate. After crack formation, the temperature distributions became irregular due to perturbed heat transfer by cracks and the influence of latent heat for moisture vaporization.

CONCLUSIONS

A finite element based method was developed to simulate heat and moisture transfer, hygrostrain–stress formation, stress crack formation and propagation in an infinitely cylindrical, elastoplastic food. Simultaneous heat and moisture transfer was simulated by Furuta and Hayakawa's model, hygrostrain–stress formation by the incremental method based on virtual work principle application, the stress crack formation by the critical tensile stress criterion, and the multiple stress crack propagation by the crack-tip-opening-angle criterion.

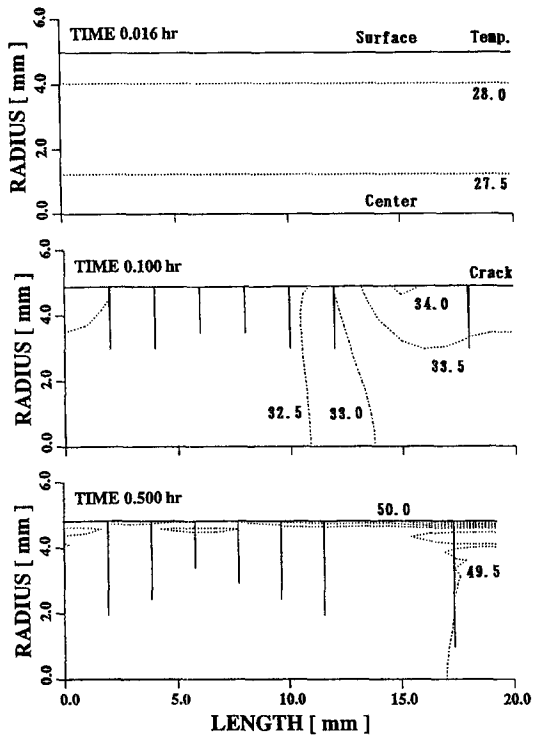

Fig. 6. Simulated temperature distributions on bisected face of a cylindrical sample made from high amylose starch powder hydrate at 0.016, 0.1 and 0.5 h of drying.

Cylindrical samples prepared from high amylose starch hydrate were subjected to forced air drying. The experimentally observed results agreed well with the simulated results.

According to the simulated results, moisture and temperature distributions were perturbed by the hygrostress crack formation and propagation. This implies that physical changes of food should be accounted for properly by accurate analysis of heat and moisture transfer.

Acknowledgements—This is publication nos D10103-1-94 and D10535-2-94 of the New Jersey Agricultural Experiment Station supported by the Center for Advanced Food Technology (CAFT), State Fund, Hatch Act Fund, National Science Foundation (supercomputer time grant at Pittsburgh Supercomputing Center), Cray Research Inc. (supercomputer time grant at Pittsburgh Supercomputing Center), and Rutgers University Computing Services. The Center for Advanced Food Technology is a New Jersey Commission on Science and Technology.

REFERENCES

1. R. N. Misra and J. H. Young, Numerical solution of simultaneous moisture diffusion and shrinkage during soybean drying, *Trans. ASAE* **23,** 1277–1282 (1980).
2. J. B. Litchfield and M. R. Okos, Prediction of corn kernel stress and breakage induced by drying, tempering, and cooling, *Trans. ASAE* **31,** 585–594 (1988).
3. K. Haghighi and L. J. Segerlind, Failure of biomaterials subjected to temperature and moisture gradients using the finite element method: I. Thermo-hydro viscoelasticity, *Trans. ASAE* **31,** 930–937 (1988).
4. K. Haghighi and L. J. Segerlind. Failure of biomaterials subjected to temperature and moisture gradients using the finite element method: II. Stress analysis of an isotropic sphere during drying, *Trans. ASAE* **31,** 938–946 (1988).
5. T. Tsukada, N. Sakai and K. Hayakawa, Computerized model for strain–stress analysis of food undergoing a simultaneous heat and mass transfer process. *J. Fd Sci.* 1436–1445 (1991).
6. C. Laguë and B. M. Jenkins, Modeling preharvest stress-cracking of rice kernels. I. Development of a finite element model, *Trans. ASAE* **34,** 1797–1811 (1991).
7. C. Lagüe and B. M. Jenkins, Modeling preharvest stress-cracking of rice kernels. II. Implementation and use of the model, *Trans. ASAE* **34,** 1812–1822 (1991).
8. T. Furuta and K. Hayakawa, Heat and moisture transfer with thermodynamically interactive fluxes and with volumetric changes. I. Mathematical model development and numerical solution, *Trans. ASAE* **35,** 1537–1546 (1991).
9. A. V. Luikov, *Heat and Mass Transfer in Capillary-porous Bodies*, pp. 248–259. Pergamon Press, Oxford (1987).
10. K. Hayakawa and J. S. Rossen, Isothermal moisture transfer in dehydrated food products during storage, *J. Can. Inst. Fd Sci. Technol.* **11,** 102–106 (1978).
11. N. Sakai and K. Hayakawa, Two-dimensional, simultaneous heat and moisture transfer in composite food, *J. Fd Sci.* **57,** 475–480 (1992).
12. C. J. Lomauro, A. S. Bakshi and T. P. Labuza, Evaluation of food moisture sorption isotherm equations. I. Fruit and vegetable products. *Lebensmittel-Wiss. Technol.* **18,** 111–117 (1985).
13. O. C. Zienkiewicz and I. C. Cormeau, Viscoplasticity, plasticity and creep in elastic solids—a unified numerical solution approach, *Int. J. Numer. Meth. Engng* **8,** 821–845 (1974).
14. O. C. Zienkiewicz, *The Finite Element Method*, pp. 458–469. McGraw-Hill, London (1986).
15. J. C. Newman Jr, An elastic-plastic finite element analysis of crack initiation, stable crack growth, and instability, *Fracture Mechanics Fifteenth Symposium*, ASTM STP-833, pp. 93–117. American Society for Testing and Materials (1984).
16. K. N. Shivakumar and J. H. Crews Jr, Energy dissipation associated with crack extension in an elastic-plastic material, *Engng Fract. Mech.* **26,** 319–330 (1987).
17. W. Horowitz (Ed.), *Official Method of Analysis* (12th Edn). Association of Official Analytical Chemists, Washington, DC (1980).